nature biotechnology

Conjugation site modulates the *in vivo* stability and therapeutic activity of antibody-drug conjugates

Ben-Quan Shen[1,2], Keyang Xu[1,2], Luna Liu[1], Helga Raab[1], Sunil Bhakta[1], Margaret Kenrick[1], Kathryn L Parsons-Reponte[1], Janet Tien[1], Shang-Fan Yu[1], Elaine Mai[1], Dongwei Li[1], Jay Tibbitts[1], Jakub Baudys[1], Ola M Saad[1], Suzie J Scales[1], Paul J McDonald[1], Philip E Hass[1], Charles Eigenbrot[1], Trung Nguyen[1], Willy A Solis[1], Reina N Fuji[1], Kelly M Flagella[1], Darshana Patel[1], Susan D Spencer[1], Leslie A Khawli[1], Allen Ebens[1], Wai Lee Wong[1], Richard Vandlen[1], Surinder Kaur[1], Mark X Sliwkowski[1], Richard H Scheller[1], Paul Polakis[1] & Jagath R Junutula[1]

The reactive thiol in cysteine is used for coupling maleimide linkers in the generation of antibody conjugates. To assess the impact of the conjugation site, we engineered cysteines into a therapeutic HER2/neu antibody at three sites differing in solvent accessibility and local charge. The highly solvent-accessible site rapidly lost conjugated thiol-reactive linkers in plasma owing to maleimide exchange with reactive thiols in albumin, free cysteine or glutathione. In contrast, a partially accessible site with a positively charged environment promoted hydrolysis of the succinimide ring in the linker, thereby preventing this exchange reaction. The site with partial solvent-accessibility and neutral charge displayed both properties. In a mouse mammary tumor model, the stability and therapeutic activity of the antibody conjugate were affected positively by succinimide ring hydrolysis and negatively by maleimide exchange with thiol-reactive constituents in plasma. Thus, the chemical and structural dynamics of the conjugation site can influence antibody conjugate performance by modulating the stability of the antibody-linker interface.

Antibody conjugates are generated by chemically linking a cysteine or lysine residue to potent chemotherapeutic drugs or other functional moieties by means of a variety of linkers[1–7]. Thiol-maleimide chemistry is a commonly used method, whereby a cysteine residue, either native or engineered, is used for conjugation[8–11]. Antibody conjugates for therapeutic applications must satisfy demanding criteria concerning specificity, safety and stability to achieve effective delivery of the payload to the target. All three components—antibody, linker and payload—play critical roles in defining target specificity, the degree of stability and mechanism of action, respectively. Indeed, the *in vivo* stability and efficacy of antibody conjugates can be improved by optimizing the linker[9,12,13] and by selecting the appropriate antibody and payload[14,15]. However, additional contributing factors, such as the influence of an antibody's chemical and structural properties on the neighboring conjugation site, have not been thoroughly investigated.

We chose antibody-drug conjugates (ADCs) and antibody-fluorophore conjugates (AFCs) as models to dissect the functional impact of the conjugation site on stability and biological activity. We have recently reported the generation of antibodies with cysteine residues engineered (referred to as THIOMABs) into the IgG heavy chain (HC-A114C) that provide reactive thiols for conjugation to the auristatin and maytansine classes of cytotoxic drugs[11,16]. These engineered ADCs displayed reduced liver and bone marrow toxicity compared to ADCs with the same drugs conjugated through either cysteine sulfhydryl groups activated by reducing interchain disulfide bonds or lysine side-chain amines[11,16]. Here we explored additional conjugation sites in the light chain (LC)[11], heavy chain-Fab region (HC)[11] and heavy chain-Fc region (Fc) of trastuzumab (Herceptin) to generate THIOMAB variants for coupling to thiol-reactive linkers (**Supplementary Fig. 1**).

Based on structural modeling, we selected three thio-trastuzumab variants (LC-V205C, HC-A114C and Fc-S396C) with conjugation sites differing in their local structural environments. Fc-S396C was predicted to have the highest fractional solvent accessibility, whereas both HC-A114C and LC-V205C variants were predicted to be in partially buried regions (**Fig. 1a**). The LC-V205C conjugation site appears to be located in a positively charged environment, whereas HC-A114C and Fc-S396C are in a relatively neutral environment (**Fig. 1b**). All three thio-trastuzumab variants showed cell-binding and internalization properties similar to that of native trastuzumab, indicating that the engineered cysteine residues do not alter the functional properties of the antibody (**Supplementary Fig. 2**).

To assess their relative therapeutic activity, we conjugated monomethyl auristatin E (MMAE) to the three thio-trastuzumab variants by a maleimido-caproyl-valine-citruline-*p*-amino-benzyloxy carbonyl (MC-vc-PAB) linker. The resulting ADCs are abbreviated as thio-trastuzumab-MC-vc-MMAE. Liquid chromatography–mass spectrometry (LC-MS) analysis confirmed that all three thio-trastuzumab-MC-vc-MMAE conjugates contained 1.7–1.9 drugs per antibody (**Supplementary Table 1**). Hydrophobic interaction chromatographic analysis revealed similar compositions of the

[1]Genentech Inc., 1 DNA Way, S. San Francisco, California, USA. [2]These authors contributed equally to this work. Correspondence should be addressed to J.R.J. (jagath@gene.com).

Received 8 July 2011; accepted 20 December 2011; published online 22 January 2012; doi:10.1038/nbt.2108

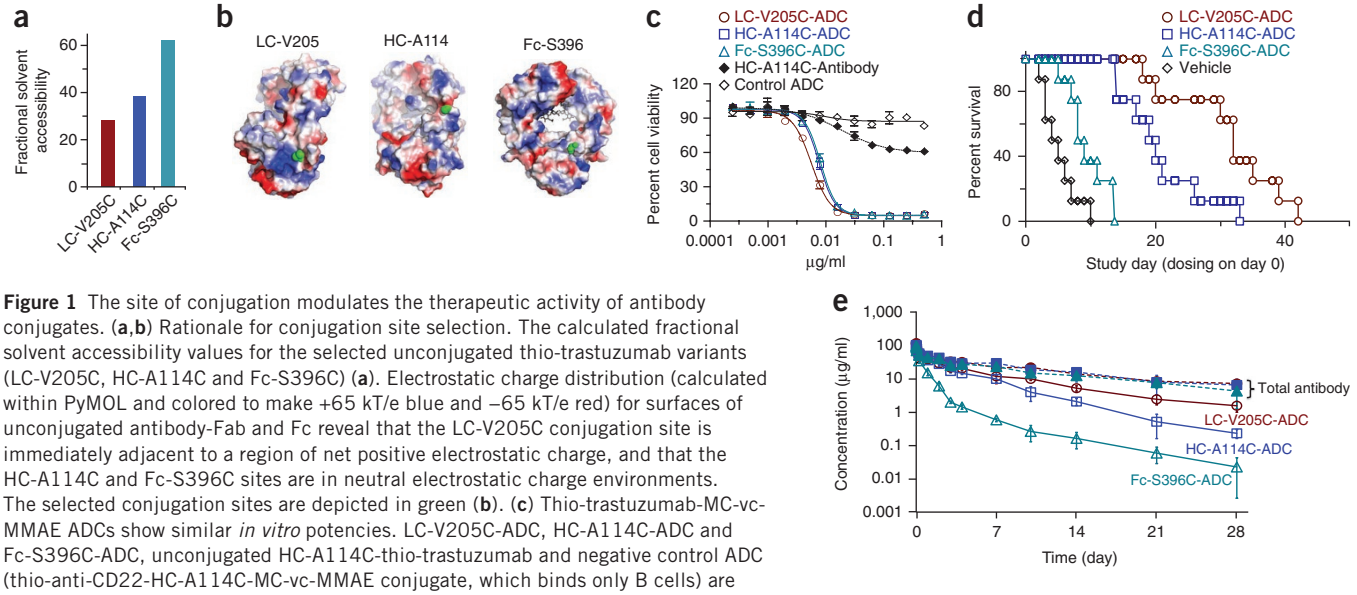

Figure 1 The site of conjugation modulates the therapeutic activity of antibody conjugates. (**a**,**b**) Rationale for conjugation site selection. The calculated fractional solvent accessibility values for the selected unconjugated thio-trastuzumab variants (LC-V205C, HC-A114C and Fc-S396C) (**a**). Electrostatic charge distribution (calculated within PyMOL and colored to make +65 kT/e blue and −65 kT/e red) for surfaces of unconjugated antibody-Fab and Fc reveal that the LC-V205C conjugation site is immediately adjacent to a region of net positive electrostatic charge, and that the HC-A114C and Fc-S396C sites are in neutral electrostatic charge environments. The selected conjugation sites are depicted in green (**b**). (**c**) Thio-trastuzumab-MC-vc-MMAE ADCs show similar *in vitro* potencies. LC-V205C-ADC, HC-A114C-ADC and Fc-S396C-ADC, unconjugated HC-A114C-thio-trastuzumab and negative control ADC (thio-anti-CD22-HC-A114C-MC-vc-MMAE conjugate, which binds only B cells) are examined for their ability to inhibit proliferation in HER2-expressing SK-BR-3 cells *in vitro*. (**d**) LC-V205C, HC-A114C and Fc-S396C ADCs differ in their *in vivo* efficacies. Kaplan-Meier plots for delayed time to progression (number of days taken for a tumor to double in size from the day of randomization or for an animal death) in response to ADC treatment. Vehicle is the formulation buffer control without ADC. The difference in time to tumor progression distributions between groups was determined using a nonparametric log-rank test, with a $P \leq 0.05$ being considered significant. Fc-S396C-ADC versus LC-V205C-ADC or HC-A114C-ADC: $P < 0.0001$; and LC-V205C-ADC versus HC-A114C-ADC: $P = 0.025$. (**e**) Equally dosed LC-V205C, HC-A114C and Fc-S396C ADCs differ in their pharmacokinetic properties in mice. At the indicated time points, blood was drawn for determination of total antibody (conjugated and unconjugated, solid symbols) and ADC (conjugated only, open symbols) levels using ELISA. The LC-V205C conjugate exhibited greater stability in the mouse plasma than the HC-A114C and Fc-S396C conjugates.

drug-to-antibody ratio (DAR) species (**Supplementary Fig. 3**). All conjugates showed similar *in vitro* potencies on a HER2-amplified breast cancer SK-BR-3 cell line (**Fig. 1c**).

We next compared *in vivo* activity using the MMTV-HER2 Fo5 trastuzumab-resistant mammary tumor model, previously shown to be responsive to trastuzumab ADCs, but not the unconjugated antibody[12]. We observed significant differences in therapeutic efficacy after a single intravenous dose of 10 mg/kg. The LC-V205C conjugate showed the greatest activity, followed by moderate activity with HC-A114C and little or no activity with Fc-S396C (**Fig. 1d**).

Because all three ADCs exhibited similar DARs, target antigen binding, internalization and *in vitro* potencies, the variation in efficacy could be due to differences in their pharmacological properties. To test this, we dosed beige nude X-linked immunodeficiency (XID) mice intravenously with LC-V205C, HC-A114C and Fc-S396C thio-trastuzumab-MC-vc-MMAE conjugates and evaluated the stability of ADCs and their corresponding antibody clearances over 28 d. Plasma samples were analyzed for ADC as well as total antibody levels using anti-MMAE antibody capture– and HER2 extracellular domain capture–based enzyme-linked immunosorbent assay (ELISA), respectively (**Supplementary Fig. 4**). The levels of the intact conjugated ADCs reflected their *in vivo* activities, with LC-V205C having the highest, HC-A114C an intermediate and Fc-S396C a minimal-to-undetectable level of the conjugate (**Fig. 1e** and **Supplementary Table 2**). However, the total antibody clearance rates for all three variants were similar, suggesting that the differences in intact ADC levels resulted from differential linker stability in plasma.

To confirm this, we incubated all three thio-trastuzumab-MC-vc-MMAE ADCs in human plasma at 37 °C in a CO_2 incubator for up to 96 h and drug loss was monitored by an affinity capture LC-MS method[17]. The LC-V205C conjugate retained a DAR of 2 throughout the 96 h incubation period (**Fig. 2a**), whereas a rapid conversion of DAR2 to DAR1 and DAR0 was observed with the Fc-S396C conjugate within 24 h. Loss of drug from the HC-A114C conjugate was intermediate to that of LC-V205C and Fc-S396C, with DAR2 remaining as the major species at 96 h (**Fig. 2b**,**c**). No changes in DAR occurred in PBS buffer over the same time period (**Fig. 2a–c**, lower panels). The heterogeneity in the Fc-S396C chromatogram at the 0 h time point and in PBS after 96 h mainly reflects in-source fragmentation during LC-MS analysis as the starting DAR species is similar to those of LC-V205C and HC-A114C by hydrophobic interaction chromatographic analyses (**Supplementary Fig. 3**) and an independent ELISA-based method (**Supplementary Fig. 5**). Thus, the rate of drug loss is dependent on the conjugation site, and the activities of the three conjugates can be ranked according to decreasing plasma stability: LC-V205C > HC-A114C >> Fc-S396C (**Fig. 2d**). To demonstrate that the Fc region *per se* was not responsible for the rapid drug loss observed with the Fc-S396C conjugate, we selected two other accessible Fc region conjugation sites, Fc-V278C and Fc-S371C (**Supplementary Fig. 1**), and tested their stability. Both conjugates were more stable than the Fc-S396C ADC, with Fc-V278C exhibiting comparable stability to HC-A114C, indicating that loss of drug is dependent on conjugation site as opposed to the antibody domain (**Fig. 2e**).

To determine whether the rate of drug loss from the antibody correlated with the production of free MMAE in plasma, we analyzed the same samples for free MMAE using LC–tandem MS (LC-MS/MS). Free MMAE levels were comparable among the three conjugates and represented <3% of the MMAE initially conjugated (**Fig. 2f**). Failure to correlate free MMAE production with drug loss from the antibody suggested different mechanism(s) other than enzymatic cleavage of the MC-vc-PAB-MMAE linker[13]. To further investigate this, the three original thio-trastuzumab variants were conjugated to the noncleavable thiol reactive linker-drugs/fluorophores; maleimido-caproyl-monomethyl auristatin F (MC-MMAF), maleimido-caproyl-Alexa488 (MC-Alexa488)

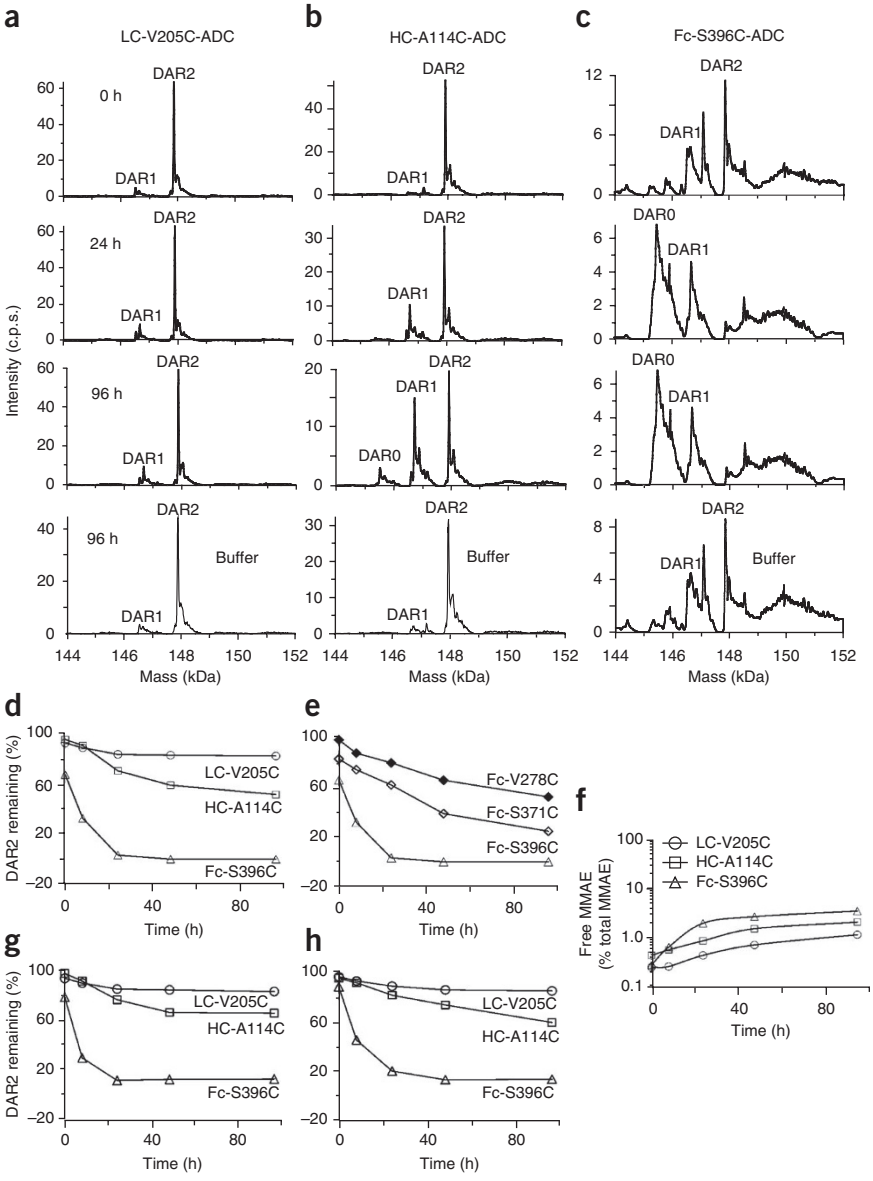

Figure 2 The plasma stability of antibody conjugates is dependent on the conjugation sites but independent of linker, drug and antibody. (**a**–**c**) Conjugation site–dependent drug loss in plasma. Representative deconvoluted mass spectra are shown here for LC-V205C-ADC (**a**), HC-A114C-ADC (**b**) and Fc-S396C-ADC (**c**). (**d**) Drug losses from the thio-trastuzumab-MC-vc-MMAE ADCs in **a**–**c** are shown as changes in the percentage of the DAR2 species with time. Percent of DAR2 was calculated by dividing the peak area of DAR2 by the sum of the peak areas of all DAR species (that is, DAR2, DAR1 and DAR0) in the ADC. (**e**) Relative ratios of DAR2 over time of thio-trastuzumab-MC-vc-MMAE conjugated in the antibody Fc region at V278C, S371C and S396C. (**f**) Loss of free MMAE does not correspond with drug released in the plasma. Free MMAE levels in plasma samples in **a**–**c** were determined using LC-MS/MS and normalized to the total MMAE conjugated to the antibody at time 0 h. (**g**) Changes of DAR2 over time in three thio-trastuzumab variants conjugated to MC-MMAF. (**h**) Similar DAR results from the ADCs with a different antibody, thio-anti-TMEFF2-MC-MMAF.

or bis-maleimido-trioxyethylene glycol-maytansinoid drug (BMPEO-DM1) and tested for plasma stability. With these non-cleavable linkers, conjugation-site dependent reduction in DAR in plasma was still observed (**Fig. 2g** and **Supplementary Figs. 6–8**). The same results were also observed when MC-MMAF was conjugated to antibody against a different target antigen (anti-TMEFF2, **Fig. 2h**), confirming that the loss of thiol-reactive linkers from the antibody is independent of drug/fluorophore, linker and target antibody.

Affinity capture LC-MS analysis revealed that DAR2 species were converted to DAR1 and DAR0 species after incubation in plasma with consistent mass shifts of ~1,200 Da observed between the different DAR species for the MC-vc-MMAE conjugates (**Fig. 3a** and **Supplementary Fig. 9**), ~810 Da for the MC-MMAF conjugates (**Supplementary Fig. 9**) and ~580 Da for the MC-Alexa488 conjugates (**Fig. 3b**). These mass shifts are consistent with a loss of thiol-reactive linkers from the antibody conjugate around the succinimide ring of the linker and followed by a possible addition of cysteine to the antibody to form a disulfide bond (**Supplementary Fig. 10**).

We propose the following model for the impact of conjugation site on the stability and *in vivo* activity of the antibody conjugates (**Fig. 3c**). The rate of conjugate clearance *in vivo* is both a function of catabolism (degradation) and deconjugation of thiol-reactive linkers in the plasma. Maleimide exchange and succinimide ring hydrolysis in the conjugated linker have been reported for protein conjugates[18,19], and albumin-MC-MMAF adducts in plasma were observed in the case of an anti-CD30-MC-MMAF conjugate[18]. In the proposed model, conjugation sites with high solvent accessibility (e.g., Fc-S396C), linker-maleimide exchange might occur rapidly from the antibody to albumin, cysteine or glutathione in the plasma. On the other hand, LC-V205C-type conjugation sites that are surrounded by a positively charged environment might rapidly undergo succinimide ring hydrolysis in the linker, thereby preventing further linker-maleimide exchange and enabling stability. The stabilized conjugate showed improved efficacy, whereas the conjugate with rapid drug loss showed decreased *in vivo* activity (**Fig. 1**).

To confirm the above-described model experimentally, we incubated LC-V205C-MC-Alexa488 (LC-V205C-AFC) and Fc-S396C-MC-Alexa488 (Fc-S396C-AFC) in human plasma for 96 h followed by size-exclusion chromatographic (SEC) analysis by monitoring Alexa488 fluorescence. Most of the LC-V205C-AFC fluorescence remained unchanged, whereas Fc-S396C-AFC lost most of its antibody-conjugate fluorescent peak with a new peak appearing at a lower molecular weight (**Fig. 3d**,**e**) identified by LC-MS as an albumin-MC-Alexa488 adduct. Similar formation of albumin-MC-MMAF or albumin-MC-vc-MMAE adducts was observed upon incubation of the corresponding ADCs in plasma. Overall, the Fc-S396C conjugate showed the highest albumin adduct formation and the LC-V205C conjugate showed very little (**Supplementary Figs. 11** and **12**). This maleimide exchange was also observed from antibody-MC-vc-MMAE to cysteine or glutathione if incubated with excess cysteine or glutathione (**Supplementary Fig. 13**).

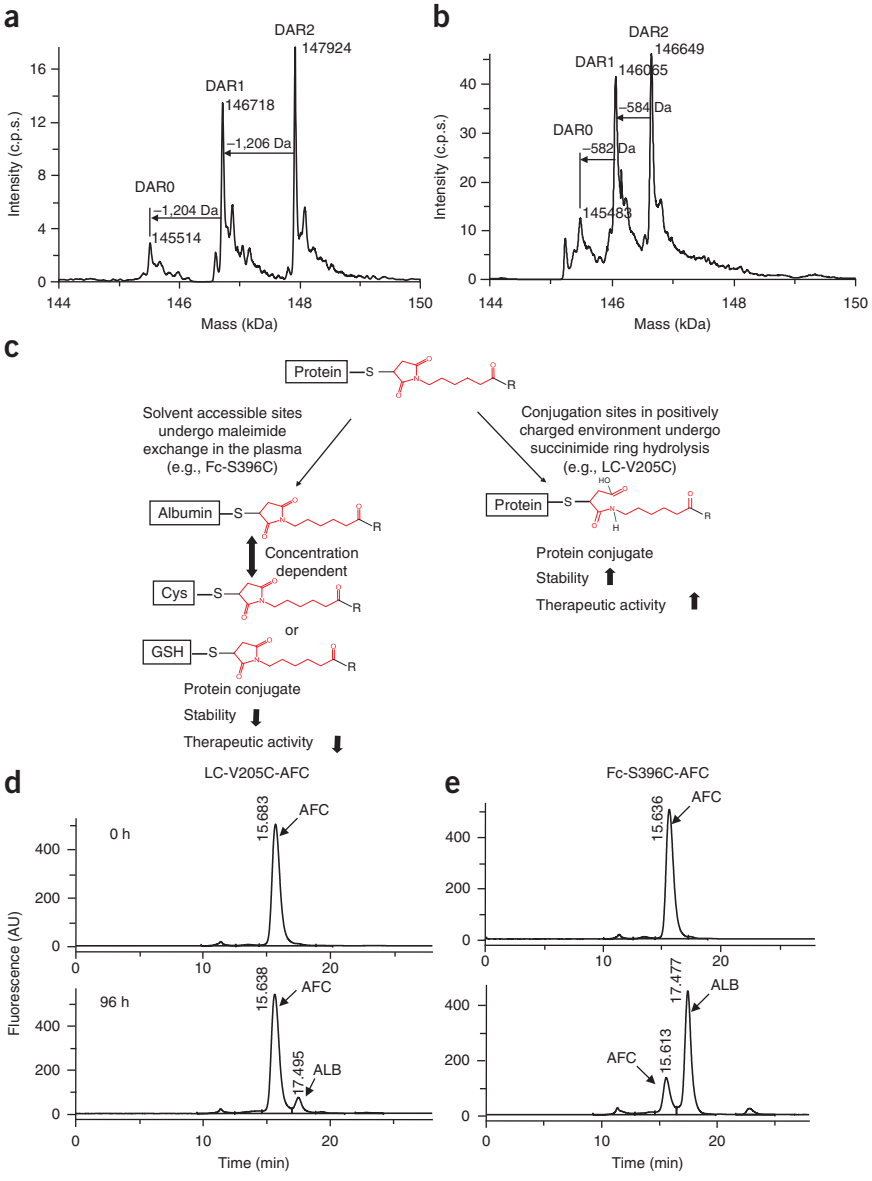

Figure 3 Proposed mechanism for the influence of the conjugation site on linker stability and therapeutic activity of antibody conjugates. (**a**,**b**) Consistent mass decreases are associated with each linker-drug loss observed from HC-A114C-MC-vc-MMAE (**a**, ~1,200 Da) or HC-A114C-MC-Alexa488 (**b**, ~580 Da) conjugates in the plasma. Antibody conjugates were incubated in human plasma at 37 °C for 96 h and the samples were analyzed by affinity capture LC-MS to determine the corresponding molecular weights of the ADC or AFC species upon drug/fluorophore loss in the plasma. (**c**) The maleimide exchange from the antibody conjugate and hydrolysis of succinimide ring in the linker are key steps that influence conjugate stability and therapeutic activity. (**d**,**e**) Linker-drug/fluorophore exchange from antibody conjugates to albumin in the plasma. SEC profiles for LC-V205C-MC-Alexa488 (**d**) and Fc-S396-MC-Alexa488 (**e**) after incubation in human plasma at 0 and 96 h. There was minimal Alexa488 transfer from the LC-V205C-MC-Alexa488 conjugate to albumin (ALB), whereas significant exchange between the Fc-S396C-MC-Alexa488 conjugate and ALB occurred. AU, arbitrary unit.

Additional inspection of the light chain from the LC-V205C-MC-vc-MMAE conjugate incubated in the plasma revealed the formation of a peak with an increase of 18 Da indicating the addition of a water molecule upon hydrolysis of a succinimide ring (data not shown). To study the effect of the hydrolyzed succinimide ring on the maleimide exchange, we incubated albumin-MC-vc-MMAE carrying both nonhydrolyzed and hydrolyzed forms of succinimide ring with excess cysteine. The data suggest that the succinimide ring, once hydrolyzed, no longer undergoes the maleimide exchange process, effectively stabilizing the conjugates (**Supplementary Fig. 14**). Moreover, the rate of succinimide ring hydrolysis in the LC-V205C conjugate was faster than that of the HC-A114C and Fc-S396C conjugates, consistent with the greater stability of the LC-V205C conjugate (**Supplementary Fig. 15**). We also observed a synergistic pH-dependent increase in succinimide ring hydrolysis (**Supplementary Fig. 15**).

The site-dependent stability seen *in vitro* with antibody conjugates was also observed *in vivo*. Plasma samples from beige nude XID mice dosed intravenously with LC-V205C, HC-A114C and Fc-S396C thio-trastuzumab-MC-vc-MMAE conjugates were evaluated by affinity capture LC-MS. Comparable to *in vitro* plasma stability, drug loss from the LC-V205C conjugate was minimal relative to HC-A114C and Fc-S396C with the latter conjugate again exhibiting the fastest rate of drug loss (**Fig. 4a**).

We also analyzed plasma samples from cynomolgus monkeys that received a single intravenous dose of anti-MUC16-MC-vc-MMAE or anti-CD22-MC-MMAF (both HC-A114C THIOMAB variants). The conjugates showed similar drug deconjugation profiles (**Fig. 4b**,**c**), confirming that the drug loss from the antibody *in vivo* was again independent of linker, drug or antibody. Analysis of the anti-CD22-MC-MMAF plasma samples beyond day 35 after dosing revealed no further loss of drug, indicating the maleimide exchange process reached a plateau after this time point (**Fig. 4d**). Moreover, the masses of the DAR1 and DAR2 species on day 35 had increased by 17 Da and 33 Da (due to hydrolysis of succinimide ring at two conjugation sites), respectively, indicating the linker succinimide ring hydrolysis had approached completion (**Supplementary Fig. 16**). Because of limited mass resolution for intact antibodies, the results of succinimide ring hydrolysis could be reflected only as increases of the average molecular weights. In the study described above for beige nude XID mice dosed intravenously with LC-V205C, HC-A114C and Fc-S396C thio-trastuzumab-MC-vc-MMAE conjugates, the rate of succinimide ring hydrolysis in the LC-V205C conjugate *in vivo* was ~13-fold faster than HC-A114C conjugate (**Fig. 4e**). Thus, the higher stability and superior *in vivo* efficacy of the LC-V205C conjugate may be due to faster succinimide ring hydrolysis, which prevents drug loss by maleimide exchange from the antibody to thiol-reactive constituents in the plasma.

In summary, we have found that the structural and chemical environment surrounding the conjugation site determines succinimide ring dynamics in the linker, where highly solvent-accessible sites are

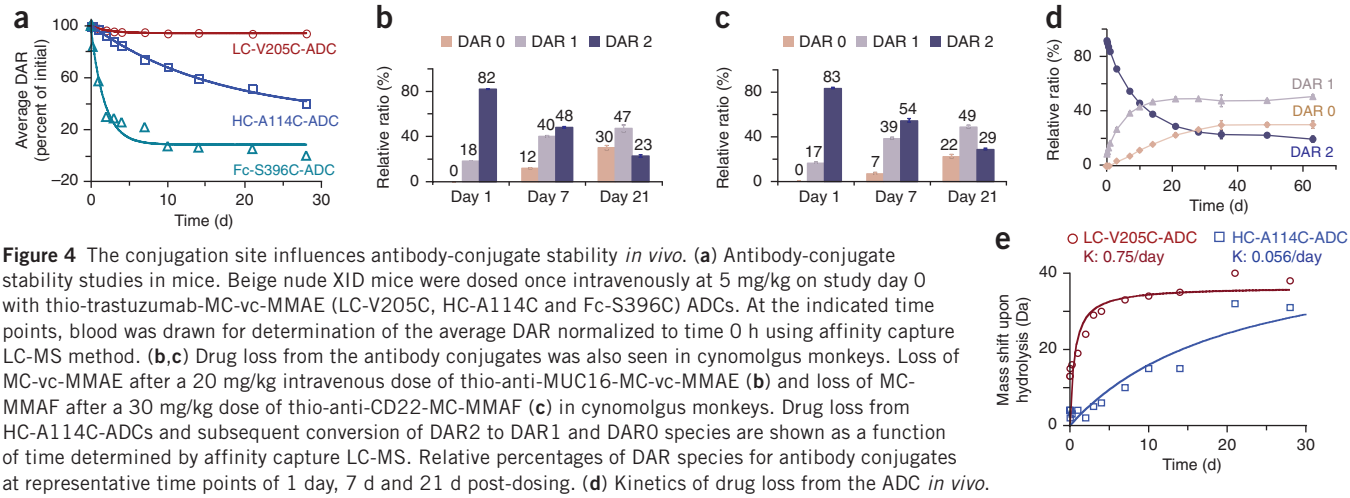

Figure 4 The conjugation site influences antibody-conjugate stability *in vivo*. (**a**) Antibody-conjugate stability studies in mice. Beige nude XID mice were dosed once intravenously at 5 mg/kg on study day 0 with thio-trastuzumab-MC-vc-MMAE (LC-V205C, HC-A114C and Fc-S396C) ADCs. At the indicated time points, blood was drawn for determination of the average DAR normalized to time 0 h using affinity capture LC-MS method. (**b**,**c**) Drug loss from the antibody conjugates was also seen in cynomolgus monkeys. Loss of MC-vc-MMAE after a 20 mg/kg intravenous dose of thio-anti-MUC16-MC-vc-MMAE (**b**) and loss of MC-MMAF after a 30 mg/kg dose of thio-anti-CD22-MC-MMAF (**c**) in cynomolgus monkeys. Drug loss from HC-A114C-ADCs and subsequent conversion of DAR2 to DAR1 and DAR0 species are shown as a function of time determined by affinity capture LC-MS. Relative percentages of DAR species for antibody conjugates at representative time points of 1 day, 7 d and 21 d post-dosing. (**d**) Kinetics of drug loss from the ADC *in vivo*. Detailed time profiles of relative percentages of DAR species for HC-A114C-ADC (that is, thio-anti-CD22-MC-MMAF) up to 63 d post-dose at 30 mg/kg of single intravenous dose in cynomolgus monkeys. Drug loss through deconjugation was minimal or essentially stopped beyond day 35 post-dose. (**e**) Hydrolysis of succinimide ring in the linker *in vivo* is faster with LC-V205C ADC compared with HC-A114C ADC. Plasma samples analyzed were from the same ADC groups as in **Figure 4a**. Increased mass shifts were calculated by subtracting the initial total mass of the ADC from the LC-MS–derived mass at the experimentally measured time points. The data was plotted in increased mass shift versus time (days). The LC-V205C-ADC seemed to undergo succinimide ring hydrolysis at least 13-fold faster than that of HC-A114C-ADC *in vivo*.

susceptible to a maleimide exchange process with albumin, cysteine or glutathione both *in vitro* and *in vivo*. In contrast, sites surrounded by positively charged amino acid residues undergo rapid succinimide ring hydrolysis in the linker, which precludes such maleimide exchange resulting in increased stability, and thereby, enhanced therapeutic activity (**Fig. 1d**). This mechanism is applicable to a number of different antibody conjugates with both cleavable and noncleavable linkers (**Supplementary Fig. 17**). A preliminary safety study in rats indicated that conjugates with rapid loss of cytotoxic drug due to the maleimide exchange process showed increased liver toxicity compared to the more stable conjugates (**Supplementary Fig. 18**). Given the limited number of constructs that we could analyze in this study we cannot rule out that in addition to solvent accessibility and charged residue environments, other structural and chemical properties such as neighboring proton donors/acceptors from protein or conjugated linkers and local protein conformation may also contribute to the linker stability. The stability of other thiol-reactive linkers such as bromoacetamide/iodoacetamide linkers may differ from that of cysteine-maleimide linker chemistry.

Maleimide is known to undergo alkaline hydrolysis, preventing conjugation to thiol groups[20,21]. Succinimide ring hydrolysis is also known to be catalyzed by bases[22]. However, the impact of succinimide ring hydrolysis on antibody conjugate stability and therapeutic activity has, to our knowledge, not been described before and might have important implications for antibody conjugate therapeutics. Although we have validated conjugation site–dependent maleimide exchange and succinimide ring hydrolysis only in antibody conjugates, it is reasonable to believe that the same rules would also apply to other protein conjugates. Our results demonstrate that the structural and chemical dynamics of the conjugation site can thus be exploited to design optimal protein conjugates for therapeutic and research applications.

METHODS

Methods and any associated references are available in the online version of the paper at http://www.nature.com/naturebiotechnology/.

Note: Supplementary information is available on the Nature Biotechnology website.

ACKNOWLEDGMENTS

We thank our Genentech colleagues: J. Speer and E. Wu for reagent generation and inventory; D. Bumbaca for plasma stability study; J. Lau and I. Inigo for ADC efficacy studies; P. Carter and S. Panowski for critical review of the manuscript; H.B. Lowman, S. Kenkare-Mitra and I. Mellman for their insightful discussions. Anti-MMAE mouse monoclonal antibodies were a generous gift from Seattle Genetics.

AUTHOR CONTRIBUTIONS

B.-Q.S. and K.X. designed experiments developed the methodology, performed plasma stability studies and wrote the manuscript. L.L. and M.K. performed plasma stability and LC-MS analyses. H.R. conducted ADC conjugations and S.B. generated THIOMAB constructs and performed *in vitro* potency studies. K.L.P.-R., J.T. and S.-F.Y. performed *in vivo* efficacy studies. E.M., D.L. and J.T. conducted pharmacokinetic studies. J.B. and O.M.S. quantified free MMAE levels in the plasma. S.J.S. performed internalization studies. P.J.M. and P.E.H. purified antibodies. C.E. performed antibody structural analysis. T.N., W.A.S., R.N.F. and K.M.F. designed and conducted preclinical safety studies. D.P. and S.D.S. provided project management support. L.A.K., A.E., W.L.W., R.V., S.K., M.X.S. and R.H.S. provided direction and guidance. P.P. provided direction, guidance and assisted in writing the manuscript. J.R.J. led the overall conjugation site-dependent antibody conjugate program, generated trastuzumab THIOMAB constructs, designed experiments and wrote the manuscript.

COMPETING FINANCIAL INTERESTS

The authors declare competing financial interests: details accompany the full-text HTML version of the paper at http://www.nature.com/naturebiotechnology.

Published online at http://www.nature.com/naturebiotechnology/.
Reprints and permissions information is available online at http://www.nature.com/reprints/index.html.

1. Carter, P.J. & Senter, P.D. Antibody-drug conjugates for cancer therapy. *Cancer J.* **14**, 154–169 (2008).
2. Polakis, P. Arming antibodies for cancer therapy. *Curr. Opin. Pharmacol.* **5**, 382–387 (2005).
3. Kreitman, R.J. & Pastan, I. Immunotoxins for targeted cancer therapy. *Adv. Drug Deliv. Rev.* **31**, 53–88 (1998).
4. Marik, J. & Junutula, J.R. Emerging role of immunoPET in receptor targeted cancer therapy. *Curr. Drug Deliv.* **8**, 70–78 (2011).
5. Ryan, S.M., Mantovani, G., Wang, X., Haddleton, D.M. & Brayden, D.J. Advances in PEGylation of important biotech molecules: delivery aspects. *Expert Opin. Drug Deliv.* **5**, 371–383 (2008).
6. McCarron, P.A. *et al.* Antibody conjugates and therapeutic strategies. *Mol. Interv.* **5**, 368–380 (2005).
7. Medintz, I.L., Uyeda, H.T., Goldman, E.R. & Mattoussi, H. Quantum dot bioconjugates for imaging, labelling and sensing. *Nat. Mater.* **4**, 435–446 (2005).

8. Hamblett, K.J. *et al.* Effects of drug loading on the antitumor activity of a monoclonal antibody drug conjugate. *Clin. Cancer Res.* **10**, 7063–7070 (2004).
9. Polson, A.G. *et al.* Antibody-drug conjugates for the treatment of non-Hodgkin's lymphoma: target and linker-drug selection. *Cancer Res.* **69**, 2358–2364 (2009).
10. Chapman, A.P. *et al.* Therapeutic antibody fragments with prolonged in vivo half-lives. *Nat. Biotechnol.* **17**, 780–783 (1999).
11. Junutula, J.R. *et al.* Site-specific conjugation of a cytotoxic drug to an antibody improves the therapeutic index. *Nat. Biotechnol.* **26**, 925–932 (2008).
12. Lewis Phillips, G.D. *et al.* Targeting HER2-positive breast cancer with trastuzumab-DM1, an antibody-cytotoxic drug conjugate. *Cancer Res.* **68**, 9280–9290 (2008).
13. Doronina, S.O. *et al.* Development of potent monoclonal antibody auristatin conjugates for cancer therapy. *Nat. Biotechnol.* **21**, 778–784 (2003).
14. Chari, R.V.J. Targeted cancer therapy: conferring specificity to cytotoxic drugs. *Acc. Chem. Res.* **41**, 98–107 (2008).
15. Wu, A.M. & Senter, P.D. Arming antibodies: prospects and challenges for immunoconjugates. *Nat. Biotechnol.* **23**, 1137–1146 (2005).
16. Junutula, J.R. *et al.* Engineered thio-trastuzumab-DM1 conjugate with an improved therapeutic index to target human epidermal growth factor receptor 2-positive breast cancer. *Clin. Cancer Res.* **16**, 4769–4778 (2010).
17. Xu, K. *et al.* Characterization of intact antibody-drug conjugates from plasma/serum in vivo by affinity capture capillary liquid chromatography-mass spectrometry. *Anal. Biochem.* **412**, 56–66 (2011).
18. Alley, S.C. *et al.* Contribution of linker stability to the activities of anticancer immunoconjugates. *Bioconjug. Chem.* **19**, 759–765 (2008).
19. Lin, D., Saleh, S. & Liebler, D.C. Reversibility of covalent electrophile-protein adducts and chemical toxicity. *Chem. Res. Toxicol.* **21**, 2361–2369 (2008).
20. Knight, P. Hydrolysis of p-NN′-phenylenebismaleimide and its adducts with cysteine. Implications for cross-linking of proteins. *Biochem. J.* **179**, 191–197 (1979).
21. Khan, M.N. Kinetics and mechanism of the alkaline hydrolysis of maleimide. *J. Pharm. Sci.* **73**, 1767–1771 (1984).
22. Kalia, J. & Raines, R.T. Catalysis of imido group hydrolysis in a maleimide conjugate. *Bioorg. Med. Chem. Lett.* **17**, 6286–6289 (2007).

ONLINE METHODS

Engineering site-specific antibody conjugates. Construction and production of the THIOMAB variants of anti-MUC16 and trastuzumab were reported previously[11,16]. Briefly, a cysteine residue was engineered at alanine 114 (Kabat numbering) of the heavy chain (in trastuzumab, anti-MUC16, anti-CD22 and anti-TMEFF2 antibodies) to produce the HC-A114C variant of THIOMAB. Similarly, a cysteine residue was engineered at valine 205 (Kabat numbering) of the light chain (trastuzumab and anti-TMEFF2) to produce the LC-V205C variant. The Fc-S396C THIOMAB variant (trastuzumab, anti-CD22 and anti-TMEFF2) was generated by engineering a cysteine residue at serine 396 (Kabat numbering) of the heavy chain. Desired linker-drug/fluorophores were conjugated and the antibody conjugates purified as described earlier[11].

***In vitro* binding, internalization and cell viability assays.** For quantitative uptake, trastuzumab and its THIOMAB variants were labeled at a 1:3 ratio with Alexa488 anti human Fc Fabs (Molecular Probes Z25402 Zenon kit), and diluted to 1 μg/ml in carbonate-free media without addition of mouse IgG block. After 1 h incubation with MCF7-HER2 cells in 6-well dishes (two independent plates per sample) on ice, cells were washed three times in ice-cold carbonate-free medium and chased for 0, 1 or 3 h in cell culture medium at 37 °C. Cells were washed twice in cold carbonate-free medium (once without and once with 10% FBS), once in PBS, then detached in 0.5 ml of 5 mM EDTA in PBS. Total (unquenched) samples were collected by centrifugation and resuspended in 2% paraformaldehyde in PBS buffer for fluorescence-activated cell sorting (FACS) analysis. Surface signal was quenched in 200 μl of 25 μg/ml rabbit anti-Alexa488 (Molecular Probes/Invitrogen A11094) in complete carbonate-free medium for 1 h on ice before fixation to determine the amount internalized. The amount internalized was expressed as a percentage of the amount bound, after subtraction of background unquenchable signal and correcting for any losses in binding during the chase, as previously described[23]. Flow cytometric analysis was performed on a FACS Calibur machine. Cell viability assays in the presence of trastuzumab ADCs (0–10 μg/ml) were carried out in SK-BR-3 cells in a 96-well format as described previously[12].

***In vitro* plasma stability studies.** Plasma (lithium-heparin) samples (human, rat, mouse and cynomolgus monkey) were purchased from Bioreclamation. Plasma was thawed, spun at 157*g* (Eppendorf centrifuge 5810R) for 5 min followed by filtration through a 0.22 μm filter (Pall Co) into sterile polypropylene tubes and kept on ice. PBS buffer was filtered and kept on ice. Conjugate stock solutions were added to selected plasma samples at a final concentration of 100 μg/ml. PBS with 0.5% BSA was used as a control. Aliquots of 100 μl from each mixture were transferred into silated microcentrifuge tubes and incubated at 37 °C in a CO_2 incubator. This allowed us to keep the plasma pH levels close to the physiological pH of 7.2 throughout the incubation period. To stop the reaction, samples were transferred to a −80 °C freezer at predetermined time points (0, 8, 24, 48 and 96 h). The 0 h collection was put on dry ice within the first minute after the conjugate addition. Samples were stored at −80 °C freezer until further analysis.

LC-MS/MS to assess the MMAE concentration in the plasma matrices. Plasma samples (25 μl per sample) were extracted by protein precipitation using 100 μl of methanol containing 0.5 nM of MMAE-d8 (deuterated internal standard). The samples were analyzed for MMAE concentrations using LC-MS/MS. The autosampler was a CTC PAL System (Leap Technologies) equipped with a cooling stack set at 4 °C. The LC system consisted of a Shimadzu SCI-10A vp system controller with two Shimadzu LC-10AD vp pumps. The analytical column (Phenomenex Synergi MAX-RP 80A, 4 μm, 50 × 2 mm) was heated to 50 °C using a Short Hot Pocket (Thermo-Fisher). The mobile phase consisted of 5 mM ammonium acetate and 0.1% formic acid in H_2O as solvent A and 5 mM ammonium acetate and 0.1% formic acid in 95:5 acetonitrile:H_2O as solvent B. A typical gradient was used. The mass spectrometer used was an API 3000 (AB Sciex) equipped with a turbo ion spray source with an HSID interface (Ionics). Multiple reaction monitoring was applied with transitions 718.5/152.2 for MMAE and 726.6/152.1 for MMAE-d8, respectively. The data were analyzed using Analyst 1.4.2 software (AB Sciex). The standard curve had a linear range from 0.049 nM to 25.0 nM for plasma samples, and 0.195 nM to 25.0 nM for the buffer samples.

SEC-HPLC. (SEC)-HPLC was done using a TSKgel G3000SW_{XL} 7.8 mm ID × 300 mm, 5 μm column (Tosch Biosciences). The mobile phase was 15% isopropyl alcohol in 0.2 M potassium phosphate, 0.25 M potassium chloride buffer, pH 6.9. The flow rate was 0.5 ml/minute for a run of 28 min. The Chemstation (Agilent Technologies) was set at 1,000 units/mV, peak-width 2 s, slit 4 nm. The pressure of the HPLC module was between 65 and 75 bars. Alexa488 was detected with an in-line fluorescent detector G1321A along with a standard Agilent 1100 HPLC module system (Agilent Technologies) and a setting of excitation wavelength at 493 nm and emission wavelength at 516 nm. Quantification of peak area (AUC) was determined by manual integration of the peak (AUC*second) detected by the fluorescent detector over a given time interval using the Chemstation software. The main peak retention time of the antibody-Alexa488 conjugate was 15.6–15.7 min. Estimated molecular weights for peaks were determined using Bio-Rad protein standards.

Affinity capture LC-MS. Affinity capture LC-MS assay was carried out to determine the relative intensities of various ADC components (DAR0–DAR2) in the plasma as described earlier[17] with the following modifications. The biotinylated extracellular domain of the relevant receptor recognized by the antibody component of the ADC was immobilized onto streptavidin-coated paramagnetic beads (Invitrogen). This affinity bead system was used to capture ADCs by incubating with the plasma samples containing ADCs for ~2 h at 25 °C. Any bound ADCs were then isolated, washed and deglycosylated on the beads in HBS-EP buffer (GE Healthcare) overnight. Subsequently, the beads were washed extensively and the ADC analytes were eluted in 30% acetonitrile in water with 1% formic acid for LC-MS analysis. A volume of 10 μl of the ADC solution was injected onto a PLRP-S column (50 × 0.3 mm, 5 μM, 4,000 Å) with a 15 μl/min flow rate. Typical mobile phase (acetonitrile and water containing 0.1% formic acid) was used. Analytes were ionized by electrospray and detected by a Q-Star XL mass spectrometer operated in the positive TOF-MS mode. Raw data of ADCs were deconvoluted using Analyst QS 1.1 software, and peak AUCs were obtained for each ADC component of interest. Relative ratios for ADC components were calculated.

***In vivo* efficacy, ADC stability and safety studies.** *Efficacy studies.* All thio-trastuzumab ADCs were tested in the Fo5 mouse mammary tumor model as described previously[12,16]. *In vivo* efficacy of thio-anti-CD22-MC-vc-MMAE (HC-A114C and Fc-S396C) ADCs were tested in a Granta-519 xenograft model of human mantle-cell lymphoma. Female C.B-17 SCID mice were subcutaneously implanted with 20 million Granta-519 cells, and dosed when the average tumor size reached 155 mm^3 (n = 10 mice/group). *In vivo* efficacy of thio-anti-TMEFF2-MC-MMAF (LC-V205C and HC-A114C) ADCs were tested in a LuCaP77 xenograft model of human prostate cancer. Male C.B-17 SCID-beige mice were subcutaneously implanted with 10–15 mm^3–sized LuCaP77 tumor fragments, and dosed when the average tumor size reached 165 mm^3 (n = 10 mice/group). All studies were conducted in accordance with the Guide for the Care and Use of Laboratory Animals.

ADC stability studies. Beige nude XID mice (n = 20/group) were administered a 5 mg/kg IV bolus dose of thio-trastuzumab-MC-vc-MMAE (LC-V205C, HC-A114C and Fc-S396C) ADCs. Blood samples were collected at selected times for up to 28 d following dosing with four animals per time point. Blood samples were processed to obtain plasma, and stored at −80 °C until analysis. The total antibody and ADC concentrations in the plasma were either quantified by ELISA (**Supplementary Fig. 3**) as described above.

Safety studies. The safety profiles for all three thio-trastuzumab-MC-vc-MMAE (LC-V205C, HC-A114C and Fc-S396C) ADCs were evaluated in rats (a nonantigen-binding animal model). Experimentally naive female Sprague-Dawley rats, ~6 weeks old (140–160 g), were purchased from Charles River Laboratories and were randomly assigned to seven groups (n = 5/group). After a week of acclimation, each group received a single intravenous (IV) bolus injection (day 1) of vehicle or each ADC at two dose levels based on drug per

doi:10.1038/nbt.2108

body surface area (1,500 and 2,635 μg MMAE/m^2 or ~30 and 50 mg/kg of antibody, respectively) as previously described[24]. Animals were monitored for 11 d with body weights measured daily and blood collected for hematology and serum chemistry analysis on days 5 and 12.

23. Austin, C.D. *et al.* Endocytosis and sorting of ErbB2 and the site of action of cancer therapeutics trastuzumab and geldanamycin. *Mol. Biol. Cell* **15**, 5268–5282 (2004).
24. Chen, Y. *et al.* Armed antibodies targeting the mucin repeats of the ovarian cancer antigen, MUC16, are highly efficacious in animal tumor models. *Cancer Res.* **67**, 4924–4932 (2007).